



ELSEVIER

Journal of Alloys and Compounds 335 (2002) 165–175

Journal of
ALLOYS
AND COMPOUNDS

www.elsevier.com/locate/jallcom

Distributions of hydrogen and strains in LaNi_5 and $\text{LaNi}_{4.75}\text{Sn}_{0.25}$

B. Fultz^{a,*}, C.K. Witham^a, T.J. Udovic^b^a*Keck Laboratory, Engineering and Applied Science, MS 138-78, California Institute of Technology, Pasadena, CA 91125, USA*^b*NIST Center for Neutron Research, National Institute of Standards and Technology, 100 Bureau Dr., MS 8562, Gaithersburg, MD 20899-8562, USA*

Received 6 July 2001; accepted 31 August 2001

Abstract

Hydrogen distributions and internal strains that accompany hydriding of binary LaNi_5 were compared to those of the ternary alloy $\text{LaNi}_{4.75}\text{Sn}_{0.25}$, which is known to have a cycle life superior to that of LaNi_5 in electrochemical cells and in gas storage applications. X-ray diffractometry shows that the unit cell volume of the hydride phase changes more continuously with hydrogen concentration in $\text{LaNi}_{4.75}\text{Sn}_{0.25}$ than in binary LaNi_5 . Gas-phase isotherms show that the Sn atoms make significant changes to the local chemical potential of hydrogen atoms. Using generic hydrogen–solite interactions in Monte Carlo simulations and physical arguments, it is shown that normal coarsening of hydride zones will be altered, or even arrested, by hydrogen–solite interactions. Small-angle neutron scattering shows that the distribution of deuterium in partially-deuterated $\text{LaNi}_{4.75}\text{Sn}_{0.25}$ is more homogeneous than in partially-deuterated LaNi_5 , at least on the spatial scales around 100 Å. It is suggested that the more homogeneous deuterium distribution in $\text{LaNi}_{4.75}\text{Sn}_{0.25}$ suppresses the strain gradients that cause decrepitation of the metal hydride. © 2002 Elsevier Science B.V. All rights reserved.

Keywords: Hydriding; Hydrogen–solite interactions; Nickel–metal hydride

1. Introduction

Compared to lead/acid batteries, developed by Planté in 1860, and nickel–cadmium batteries, developed by Edison and by Junger in 1901, nickel–metal hydride batteries are new, being proposed around 1970 but becoming practical only since the 1980s. The market for nickel–metal hydride batteries now exceeds that of nickel–cadmium, and continues to grow. The commercial success of nickel–metal hydride battery systems has occurred so quickly that some important issues affecting their performance are poorly understood, in particular the issue of capacity fade, or the gradual deterioration of the energy that can be delivered by a cell after it has undergone a few hundred charge/discharge cycles. It is well known that capacity fade originates with corrosion of the metal hydride electrode, LaNi_5 :



with a free energy change much greater than 100 kcal/mol (LaNi_5) [1,2]. It should also be pointed out that LaNi_5

is unstable in the presence of hydrogen. A disproportionation reaction:



is driven by a free energy of 26 kcal/mol [3–5]. Alloying the LaNi_5 with small amounts of solutes can reduce its free energy, helping to stabilize it against the corrosion and disproportionation reactions. Unfortunately, the free energies of these two reactions are far larger than any such stabilization by alloying. For example, alloying with 4% Sn increases the stability of the LaNi_5 by about 4 kcal/mol (using the approach of Miedema [6]). Microstructural modifications to the alloy, such as control of grain size or defect density, have even smaller effects on the free energy. It is therefore impossible to develop a LaNi_5 -based electrode that is thermodynamically stable in an alkaline cell.

The capacity fade of LaNi_5 -based electrodes is controlled by kinetics, and these kinetics can be varied greatly by solute substitution for La or Ni. Work by the groups of Sakai [2,7–10], Willems [1,11], Srinivasan and McBreen [12–14], Percheron-Guégan [15], Schlapbach [16–18], and Fultz [19–22] have shown clear effects of solute additions on the cycle life of LaNi_5 , or its misch-metal counterpart, MmNi_5 . For example, some commercial formulations of

*Corresponding author.

E-mail address: btf@hyperfine.caltech.edu (B. Fultz).

metal hydride electrode materials with good cycle life have compositions close to $Mm_1Ni_{3.5}Co_{0.8}Mn_{0.4}Al_{0.3}$. The mechanism by which these solute substitutions affect corrosion kinetics are, unfortunately, poorly understood.

There is a broad consensus that high surface areas are detrimental to corrosion resistance [1,2,7,10,23–25]. For example, Notten et al. [23,26] have demonstrated that the cycle life of metal hydride electrodes deteriorates when the metal hydride alloy comprises smaller particles. (They were careful to use particle sizes smaller than would occur after hydrogen absorption by a fresh ingot.) Others have shown a correlation between fracture or oxidation of the metal alloy and poor cycle life [27–29]. The breakup of the $LaNi_5$ into smaller particles will provide a larger surface-to-volume ratio, offering more reaction sites for corrosion. This breakup or ‘decrepitation’ is often attributed to the strains in $LaNi_5$ during hydriding, which are enormous, being 5–7%. The elastic limit of brittle $LaNi_5$ is well below 1%, and with abundant flaws in the material it seems intuitive that cracking should occur. Nevertheless, the ‘beneficial solute additions’ do not suppress the volume dilatations of hydriding anywhere near what is required to reduce the hydriding strains below the elastic limit of $LaNi_5$. Other mechanical properties such as fracture toughness are also altered by alloying [1,2,7,10,30]. The relationship between hydriding-induced strains and cycle life is not obvious, and motivated the present study.

The volume dilatation of hydriding cannot affect directly the decrepitation of the metal hydride because uniform hydrostatic pressure does not drive crack propagation. If the volume dilatation of hydriding is large, but occurs uniformly throughout the material, there can be no release of elastic energy by crack propagation. There is evidence that large, but homogeneous, dilatations allow good cycle life. In a series of experiments, the Philips group has studied hydrogen absorption in La–Ni–Cu alloys by in-situ X-ray diffractometry [24,31,32]. They varied the Ni concentration to deviate from the AB_5 stoichiometry. The off-stoichiometric alloys were shown to have: (1) sloping plateaus in absorption isotherms; (2) gradual shifts in the positions of the diffraction peaks from the α -phase and the β -phase with hydrogen concentration, and (3) much improved cycle lives when used in battery electrodes. The Philips group argued that the continuous nature of the hydriding transformation for the alloy $AB_{5.4}$ caused the interface between the α -phase and the β -phase to broaden, thus reducing the stress intensities at the α/β interface.

The present study was designed to measure both strains and hydrogen distributions in the alloys $LaNi_5$ and $LaNi_{4.75}Sn_{0.25}$. The $LaNi_{4.75}Sn_{0.25}$ alloy has been shown to have a superior cycle life to $LaNi_5$ both in gas-phase reactions [33] and in electrochemical cells [13,19–22,34–37]. Our X-ray diffractometry of hydrided materials showed that the overall volume expansions of the two alloys were approximately the same. The two materials $LaNi_5$ and $LaNi_{4.75}Sn_{0.25}$ had differences in unit cell

volumes between fully-hydrided and fully-dehydrided states that were 23 and 21%, respectively. More significant, however, was the observation of how the unit cell of the $LaNi_{4.75}Sn_{0.25}$ shrinks more continuously with dehydriding than that of $LaNi_5$. Small angle neutron scattering (SANS) measurements were performed on deuterated samples of both $LaNi_5$ and $LaNi_{4.75}Sn_{0.25}$, and showed that the deuterium distribution was more heterogeneous in partially-deuterated $LaNi_5$. By generic Monte Carlo simulations and physical arguments, we show that interactions between Sn and deuterium atoms could be responsible for homogenizing the deuterium distribution on a mesoscopic scale. Small angle neutron scattering shows that the distribution of deuterium in partially-deuterated $LaNi_{4.75}Sn_{0.25}$ is more homogeneous than in partially-deuterated $LaNi_5$, at least on the spatial scale of 40–150 Å. We suggest this more homogeneous deuterium distribution suppresses the strain gradients that cause defect formation and fracture during hydriding.

2. Experimental

2.1. Materials preparation

Several different alloys were prepared for this work. X-ray diffractometry (XRD) and isotherm measurements were obtained on all materials to ensure they were similar. Alloys were prepared at Caltech by induction melting stoichiometric amounts of La and Ni (99.99%) and annealing in argon at 950°C for 72 h. The Sn-substituted alloys used to measure pressure–composition isotherms and XRD lattice parameters were prepared in the same way by Hydrogen Consultants, Inc. The binary alloy used for SANS measurements was obtained from Alfa Aesar, certified at 99.9% purity and packed under argon. The Sn-substituted sample used for SANS analysis was prepared at Ames Lab from Belmont Sn, zone-refined Ni, and La purified to 99.99%. Ingots were prepared by arc melting, followed by annealing in argon at 950°C for 120 h. All handling after annealing was performed in an argon glove box. All materials were stored in argon-filled vials after preparation.

2.2. Sievert’s apparatus

Isotherm measurements on the binary alloy were performed with an automated Sievert’s apparatus [33], and those of the Sn-substituted alloys are from the work of Luo et al. [38,39]. Hydrogen gas of ULSI grade (99.9999%) from Matheson Gas Products was used for the isotherm studies. All gas handling equipment was constructed using 316 stainless steel components, and the MH alloys were contained in a double-walled copper reactor designed to enhance thermal conductivity. The ingots were activated

before isotherm measurement by hydrogen absorption followed by several thermally-driven absorption/desorption cycles to ensure that the surface areas of the samples were approximately steady state.

2.3. XRD procedures

X-ray diffractometry with an Inel CPS-120 diffractometer using Co K α radiation ($\lambda_{\alpha} = 1.7902 \text{ \AA}$) was performed on all alloys to check phase composition, and to measure alloy lattice parameters. To measure the lattice expansion induced by hydrogen absorption, the method of Johnson and Reilly was used to ‘poison’ the surface layers of hydrided alloys with CO [40]. Surface poisoning of the alloys was performed after hydrogen activation in the Sievert’s apparatus. The sample chamber was then sealed at high pressure, removed from the Sievert’s apparatus, and relocated to the poisoning stand, where it was immersed in liquid nitrogen. After cooling, the sample was exposed to CO at 5 atm. After the CO had condensed on the alloy surface, the liquid nitrogen was allowed to boil off, slowly bringing the sample back to room temperature. When the sample had reached room temperature, the pressure of CO in the chamber was 40–45 atm. This procedure creates a lanthanum carbonate film on the powder surface, allowing the alloys to retain their hydrogen composition when exposed to air. After the poisoning treatment, the alloys lose hydrogen slowly so that diffraction patterns could be recorded over intervals of several days, each at different hydrogen compositions. Lattice parameters were determined by Rietveld analysis using the program RIETAN-2000 [41].

2.4. SANS procedures

Small angle neutron scattering measures an intensity, I , versus scattering angle, 2θ , near the forward beam. The reciprocal space distance is $Q = 4\pi \sin(\theta)/\lambda$, where λ is the neutron wavelength (at small angles $Q = 4\pi\theta/\lambda$). The intensity $I(Q)$ can be shown to be proportional to:

$$I(\vec{Q}) \propto \int_{-\infty}^{\infty} \exp(-i\vec{Q} \cdot \vec{R}) G(\vec{R}) d^3R \quad (1)$$

where

$$G(\vec{R}) \propto \int_{-\infty}^{\infty} \Delta\rho(\vec{r}) \Delta\rho(\vec{r} + \vec{R}) d^3R \quad (2)$$

The SANS intensity $I(\vec{Q})$ reflects heterogeneities in a density, $\Delta\rho(\vec{r})$. This is the density of scattering lengths, b , of the nuclei in the object. For an isolated object, $I(\vec{Q})$ is proportional to $|b|^2$. In the present work, we seek the density variation of deuterium nuclei. Unfortunately, the metallic alloy itself also has density variations that contribute significantly to the SANS intensity. The measurements

were therefore designed to measure differences in $I(Q)$ from samples with varying amounts of deuterium. If the object of interest were large and homogeneous, $G(R)$ would extend over large R , so the Fourier transform of Eq. (1) would be a point at $Q=0$. The SANS profile would be indistinguishable from the forward beam. On the other hand, small objects have a $G(R)$ that has a shape somewhat larger than the object itself, and have intensity at larger Q .

The scattering measurements were performed on the 8-m SANS instrument at the NIST Center for Neutron Research. Incident neutron wavelengths of both 5 and 15 \AA ($\Delta\lambda/\lambda = 0.25$) were used, providing a usable Q range of 0.007–0.4 \AA^{-1} . All measurements were made at 295 K. The scattering data were corrected for background, empty-cell scattering, and pixel-by-pixel detector sensitivity. All scattering patterns had cylindrical symmetry about the forward beam, so the data were averaged over rings. The reported intensities are in absolute units based on direct beam flux measurements.

Approximately 5 g of LaNi₅ and 6 g of LaNi_{4.75}Sn_{0.25} were precycled once each in the following manner. The virgin alloy was coarsely ground in a He-filled glovebox to enhance the rate of D₂ absorption, then loaded into a stainless steel tube sealed by a Cu gasket and equipped with a gas valve. The alloy was vacuum annealed at 473 K for 1 h followed by the introduction of ≈ 0.7 MPa of D₂ gas (Cambridge Isotope Laboratories¹, 99.9% isotopic purity). The alloy was subsequently cooled to 293 K in the D₂ atmosphere and equilibrated there for ≈ 20 h. On completion of this first deuterium loading, the number of deuterium atoms absorbed per formula unit as determined by volumetric uptake measurements were 6.4 and 6.2 for LaNi₅ and LaNi_{4.75}Sn_{0.25}, respectively. The deuterium was finally removed by evacuating at 373 K for 3 h.

A 1-g portion of each precycled alloy was reloaded in the glovebox into its own stainless steel SANS cell equipped with a valve and two Viton-o-ring-sealed, quartz windows of 3.2-mm-thickness. The sample itself was a disk with a diameter of 25.4 mm and thickness of 1 mm. The alloys were fully reloaded with D by exposure to D₂ at a pressure of approximately 0.4 MPa and a temperature of 293 K. After SANS measurements, partial removal of D was accomplished by controlled evacuation of the desorbing D₂ gas at 293 K. After each such step, the cell valve was sealed, the sample quickly equilibrated, and another SANS measurement was performed. To ensure complete D removal for the last step of each complete desorption cycle (i.e. the D-free alloy), the sample was evacuated at approximately 350 K for up to 1 h. Table 1 indicates the treatment history after precycling, starting with the fully-deuterided samples used in the first SANS measurements.

¹Manufacturers are identified in order to provide complete identification of experimental conditions, and such identification is not intended as a recommendation or endorsement by NIST.

Table 1
Deuteriding and hydriding sequence for SANS measurements

First SANS desorption cycle (samples initially deuterided)				
LaNi ₅	6.4 D	4.0 D	1.6 D	0 D
LaNi _{4.75} Sn _{0.25}	6.2 D	4.0 D	1.9 D	0 D
Second SANS desorption cycle (samples initially deuterided)				
LaNi ₅	6.3 D	3.9 D	1.6 D	
LaNi _{4.75} Sn _{0.25}	6.1 D	4.1 D	1.9 D	

Hydrogen or deuterium concentration, x , in formula unit: LaNi₅D _{x} .

3. Results

3.1. Isotherms

The isotherms of the various LaNi_{5-y}Sn_y alloys are shown in Fig. 1, including data measured by Luo et al. [38,39]. Three effects can be seen with increasing composition of tin. First, the plateau pressures decrease as a result of the larger alloy lattice parameter. Second, the width (in hydrogen composition) of the isotherm decreases, a result of hydrogen blocking by tin atoms. Finally, the edges of the plateau regions, where the second phase is nucleating, become less sharp.

Because the isotherm of LaNi₅ is extremely sensitive to composition, annealing conditions, and associated atomic disorder, it can be used to test the preparation of the alloy. Low-resolution isotherms were used to confirm that the LaNi₅-X alloys of the same composition were equivalent. Additionally, isotherms of both Sn_{0.25} alloys measured by Luo et al. [39] also confirm that these alloys are almost identical in composition and atomic order.

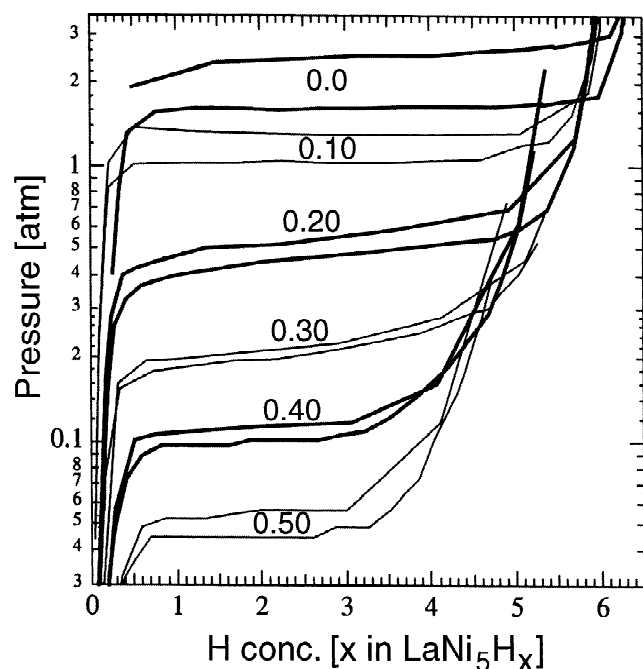


Fig. 1. Absorption and desorption isotherms of LaNi_{5-y}Sn_y alloys, with y varying from 0 to 0.5. Data for $y > 0$ are from Ref. [38].

3.2. XRD

Fig. 2a shows that the lattice parameters of the binary LaNi₅ change discontinuously with the state of hydrogenation. The set of peaks from β -phase (the hydride) shift position to higher 2θ -angles once the α -phase has begun to form, but the diffraction peaks of neither the α -LaNi₅ nor the β -phase change position once the α -phase has begun to form. With increasing time and loss of hydrogen from the sample, the intensities of diffractions from the α -phase continue to grow at the expense of those of the β -phase, but the lattice parameters of each do not change. Fig. 2b for LaNi_{4.75}Sn_{0.25} shows a different behavior. With increasing time, the diffraction peaks from the β -phase gradually undergo a large shift in position as hydrogen leaves the sample. The sample may not lose hydrogen homogeneously, perhaps owing to variations in the surface permeability, and some of the peaks are broadened or show splitting. Nevertheless, a Voigt function was fit to all peaks of the β -phase, and peak centers were used to obtain lattice parameters from pattern refinement calculations. Results

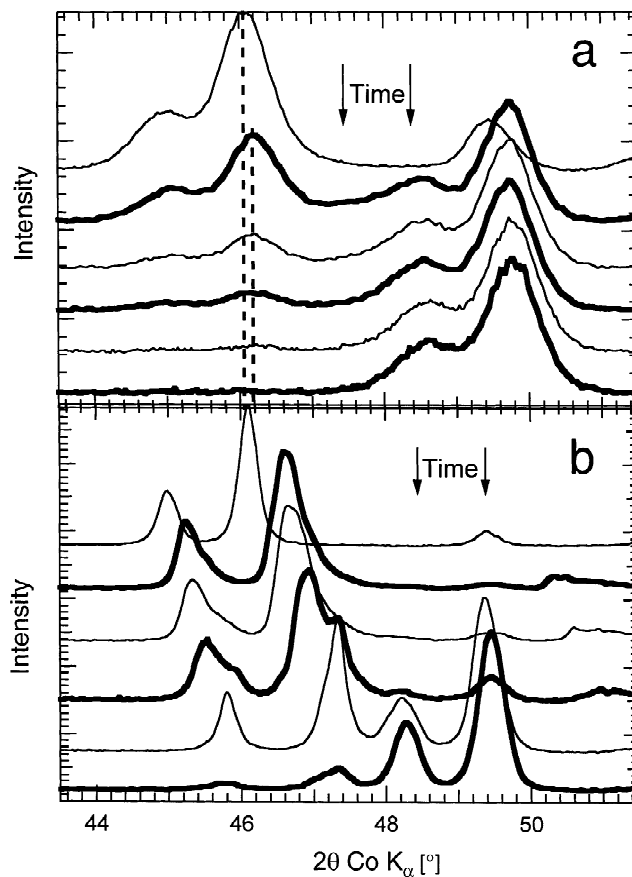


Fig. 2. X-ray diffraction patterns of: (a) binary LaNi₅ and (b) ternary LaNi_{4.75}Sn_{0.25} containing various amounts of hydrogen. In these figures, the diffraction pattern from the fully-hydrated material is at the top, and the lower patterns were measured after increasing amounts of hydrogen loss. Notice that only the β -phase of the ternary LaNi_{4.75}Sn_{0.25} alloy shows any continuous variation with hydrogen desorption.

are presented in Fig. 3. There is no linear correlation between the horizontal axis (time scale) and the hydrogen concentration, except that there is less hydrogen in the samples at later times. Fig. 3 shows that the binary alloy has very small regions where the lattice expands continuously, consistent with results from Notten et al. [32]. However, the lattice parameters of the Sn-substituted alloy initially exhibit a gradual reduction until the α -phase nucleates.

3.3. SANS

Fig. 4 shows the SANS curves from the sample of $\text{LaNi}_{4.75}\text{Sn}_{0.25}$ during its first discharge with deuterium. The data sets acquired with 5 and 15 Å neutrons cover different ranges of Q , but overlap well from $0.03 < Q < 0.1$ Å where both sets are reliable. The data show a systematic increase in intensity as deuterium is added to the material,

as expected owing to the additional scattering of deuterium. The shapes of the curves do not change significantly with deuterium concentration. A second deuterium cycle showed the same trend, but the changes in the curves with deuterium concentration were somewhat larger.

Fig. 5 compares SANS curves for fully deuterated LaNi_5 and fully deuterated $\text{LaNi}_{4.75}\text{Sn}_{0.25}$. The curves are nearly identical. The other SANS curves for LaNi_5 did not show a simple shift upwards with deuterium concentration as for $\text{LaNi}_{4.75}\text{Sn}_{0.25}$ in Fig. 4. Fig. 6 shows the SANS data for the two materials, $\text{LaNi}_{4.75}\text{Sn}_{0.25}$ and LaNi_5 , deuterated to 1/3 of their capacities. Although these curves are similar at small Q , they diverge at larger values of Q . The sample of LaNi_5 shows evidence of larger heterogeneities in deuterium concentration at small spatial scales.

Fig. 7 shows the difference when the SANS intensity from $\text{LaNi}_{4.75}\text{Sn}_{0.25}$ was subtracted from that of LaNi_5 at

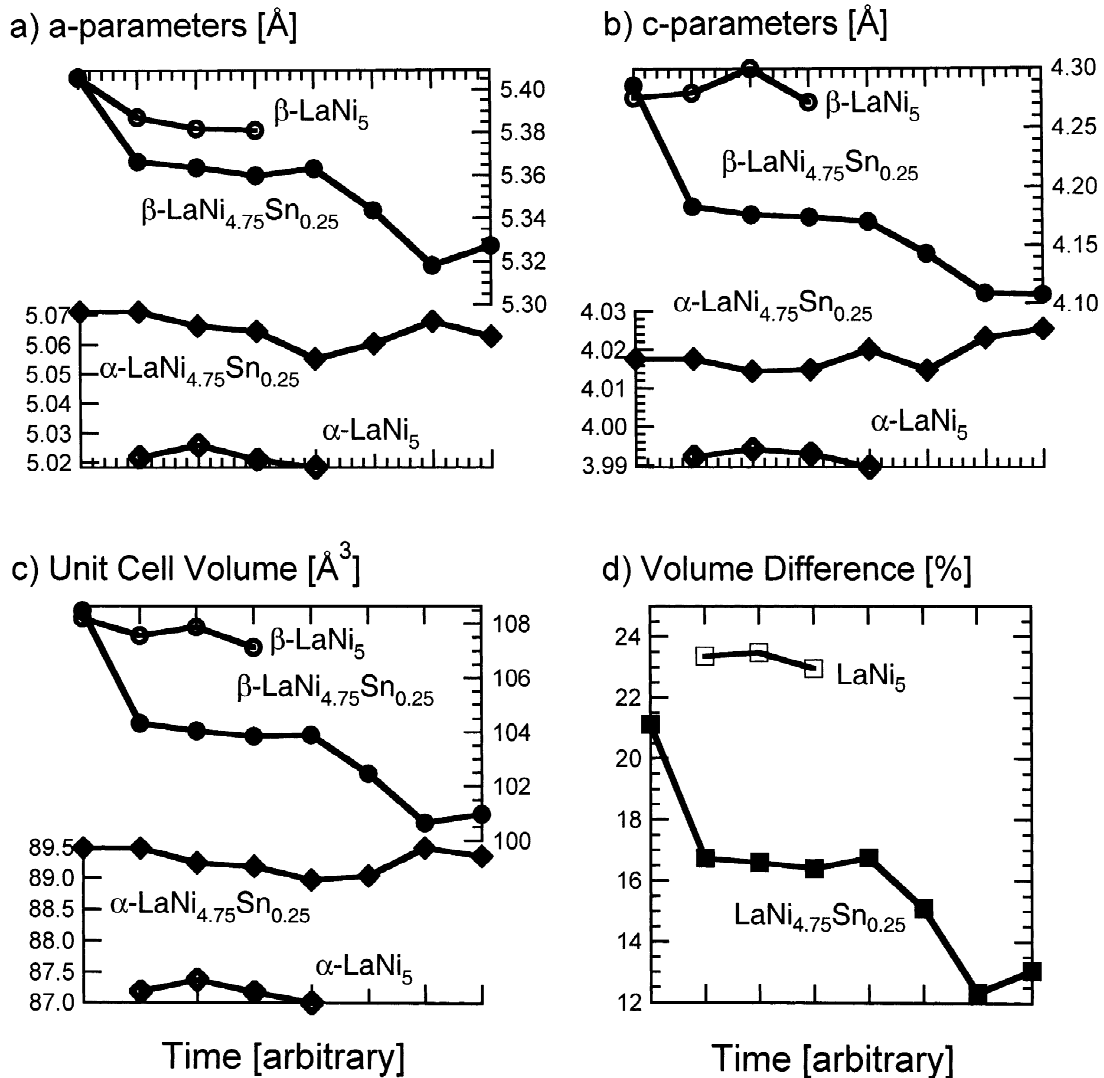


Fig. 3. X-ray lattice parameters and unit cell volume of $\text{LaNi}_{5-y}\text{Sn}_y$ versus time for hydrogen desorption; (a) a -parameter; (b) c -parameter; (c) unit cell volume; (d) fractional difference between α - and β -phase volumes.

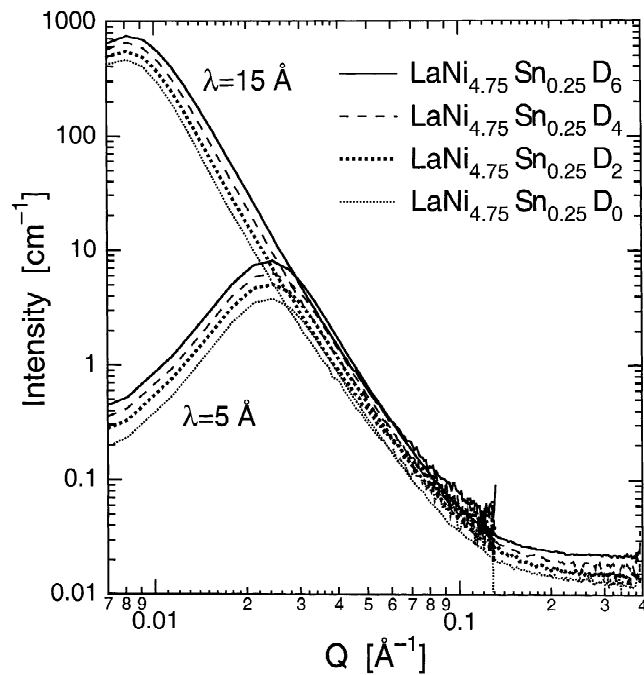


Fig. 4. Porod (log–log) plot of the measured SANS intensity from the first deuterium desorption cycle of sample of $\text{LaNi}_{4.75}\text{Sn}_{0.25}$.

the same state of deuteration. The difference is representative of the larger heterogeneity of the deuterium concentration in $\text{LaNi}_5\text{-D}$. This difference is small for the fully-deuterated samples — their curves in Fig. 5 are nearly the same. The difference between the curves in Fig. 6 for samples deuterated to 1/3 their capacity is about five

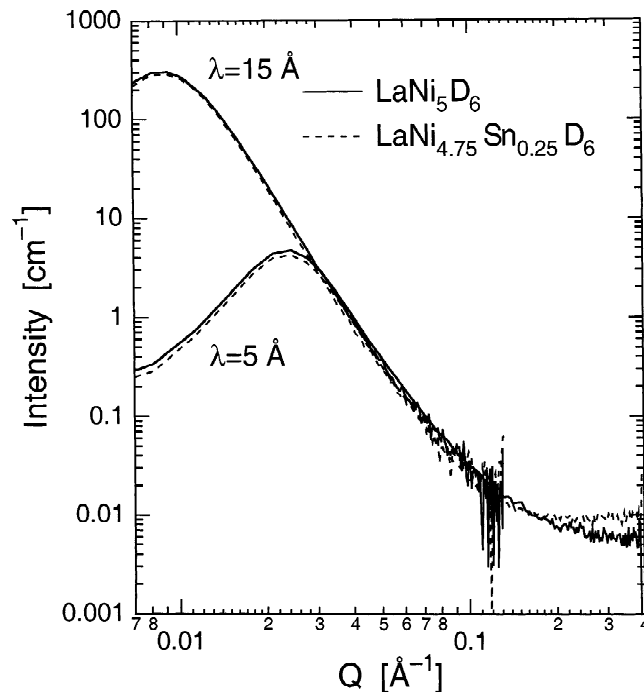


Fig. 5. Porod plot of the measured SANS intensity from the first full deuterium charging of LaNi_5 and $\text{LaNi}_{4.75}\text{Sn}_{0.25}$.

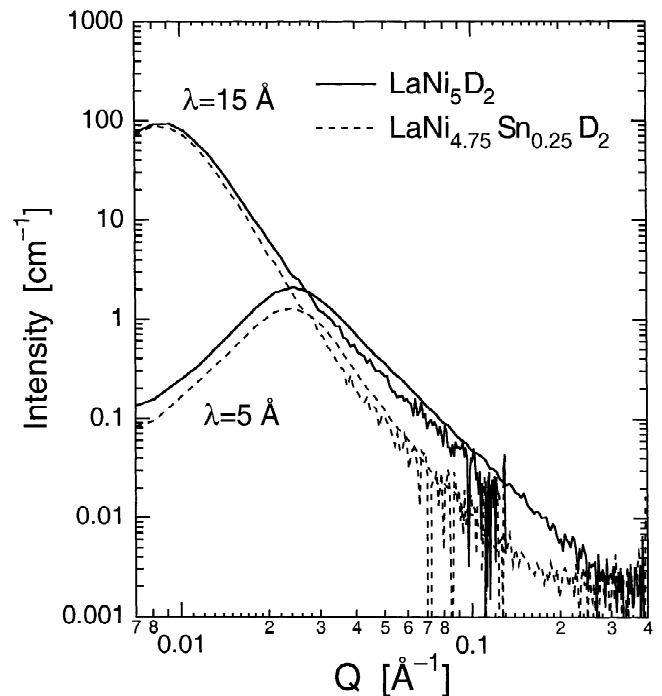


Fig. 6. Porod plot of the measured SANS intensity from the first full deuterium desorption to 33% absorption ($\text{H}/\text{unit cell}=2.0$) for LaNi_5 and $\text{LaNi}_{4.75}\text{Sn}_{0.25}$.

times larger, at least at large Q . Furthermore, the excess scattering intensity of the partially-deuterated samples of LaNi_5 has a different shape from that of the $\text{LaNi}_{4.75}\text{Sn}_{0.25}$. Similar plots were obtained by subtracting the spectra of the deuterated LaNi_5 from the undeuterated samples of LaNi_5 . Lines of slope -3 and -4 are drawn on

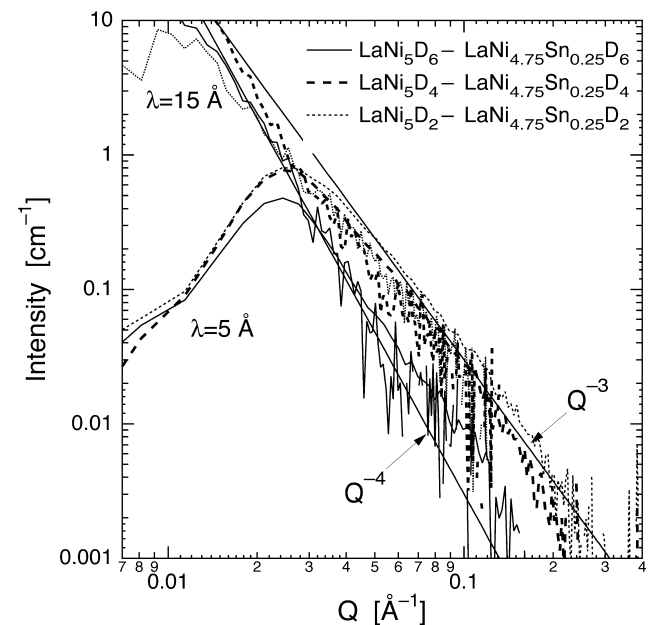


Fig. 7. Porod plot of the difference in measured SANS intensity from LaNi_5 and $\text{LaNi}_{4.75}\text{Sn}_{0.25}$ at different states of deuteration.

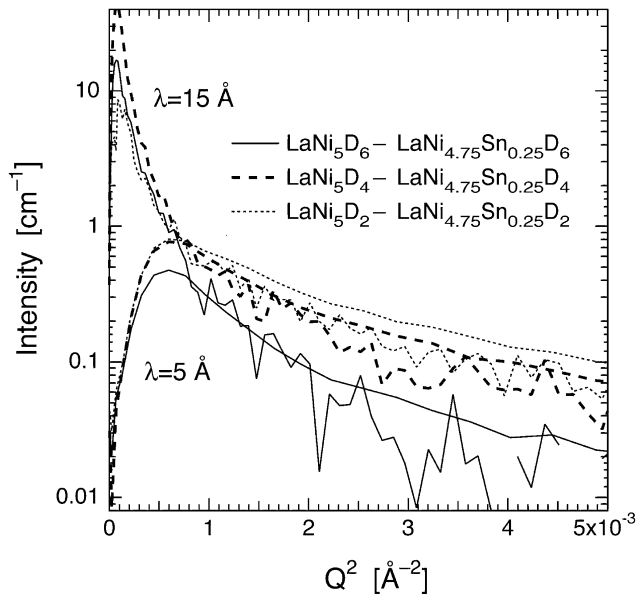


Fig. 8. Guinier plot of difference in measured SANS intensity from LaNi_5 minus that of $\text{LaNi}_{4.75}\text{Sn}_{0.25}$ at different states of deuteration.

Fig. 7, showing that the excess scattering from the sample of 1/3 or 2/3 deuterated LaNi_5 has a slope closer to -3 than -4 .

The data of Fig. 7 are plotted in Guinier form in Fig. 8. Approximate Guinier radii, r_G , were obtained from the slopes, m , of the low- Q and high- Q parts of the curves in Fig. 8 (below and above $Q^2=0.008$), as $r_G^2=3 \ln(m)$. These radii of gyration were 140 Å for the low- Q part and 44 Å for the high- Q part. These values are not accurate for several reasons, especially since $Qr_G > 1$ over at least some of these ranges, so the Guinier approximation is not reliable. Nevertheless, it seems that the excess SANS intensity from the partially-deuterated LaNi_5 arises from heterogeneities of the deuterium distribution on the order of 40–150 Å.

The SANS intensities at the minimum and maximum values of Q do not provide information on the heterogeneities of deuterium concentration. At $Q > 0.1$, the SANS curves are dominated by instrument background and incoherent scattering from hydrogen impurities or the gas. The flat part of the intensity at $Q > 0.3$ was reasonably linear with the amount of deuterium in the sample, as expected if there was a residual hydrogen concentration in the deuterium gas. At small Q the data decrease, owing to effects of the beamstop. This occurs at approximately 0.01 and 0.03 Å⁻¹ for neutrons with incident wavelengths of 15 and 5 Å, respectively.

4. Monte Carlo simulations

Two-dimensional Monte Carlo simulations were helpful for understanding how the interactions of hydrogen atoms

with a minority solute species could affect distributions of hydrogen atoms in alloys. The simulations were performed with software codes used in our previous studies on atom diffusivities in binary and ternary metallic alloys [42–44], but modified to include a sublattice for interstitial hydrogen atoms. Only hydrogen atoms were allowed to move by jumping into adjacent empty interstitial sites, using the algorithm of Metropolis et al. [45]. Interactions between hydrogen atoms were attractive over first-neighbor distances. The hydrogen atoms were either attracted or repelled by the minority solute atoms. Initial distributions of the hydrogen atoms over the interstitial sites were either random or clustered, and the evolution of the hydrogen atom distribution was monitored in time and in Monte Carlo steps [46].

An enlarged region of metal atoms plus hydrogen atoms is shown in Fig. 9a, whereas Fig. 9b,c shows only the

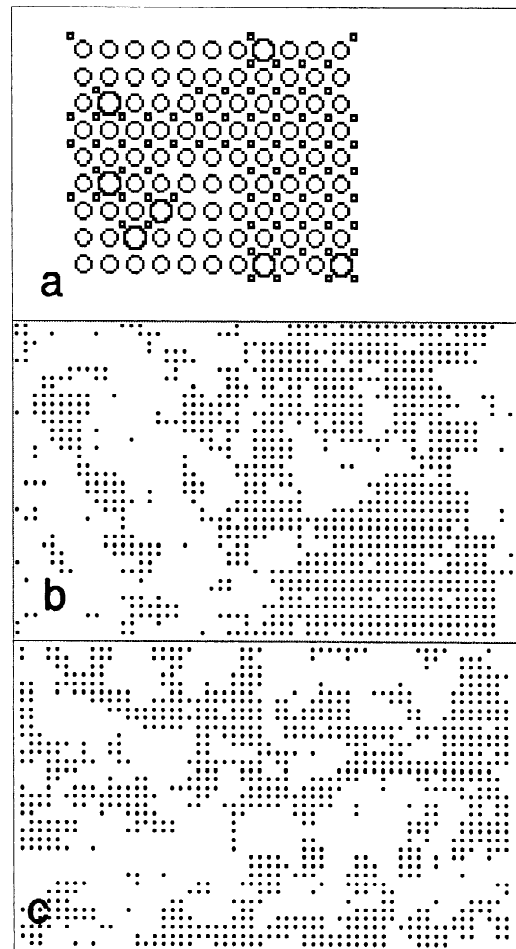


Fig. 9. (a) Typical region from simulation of part c, showing large metal atoms and small hydrogen atoms. Note preference of hydrogen atoms for the solute B-atoms (largest circles); (b) Hydrogen distributions in random alloy, $c_B=0.08$, $c_H=0.5$, $V_{A-H}=0$, $V_{B-H}=-2$ over long-range $V_{H-H}=-1.7$; (c) Hydrogen distributions in random alloy, $c_B=0.08$, $c_H=0.5$, $V_{A-H}=0$, $V_{B-H}=-1.2$, $V_{H-H}=-1.7$. Interatomic potential between hydrogen (H), metal (A), and minority solute (B) atoms are in units of kT/atom.

hydrogen atoms. The underlying metal atom lattice contained 8% minority solute atoms for all simulations, and the random metal atom arrangement was kept fixed throughout all simulations. Fig. 9b shows the hydrogen distribution (after an intermediate time) for the case where all metal atoms had no interactions with hydrogen atoms. The clustering of hydrogen for this case proceeded with normal kinetics, where the length of the characteristic hydrogen clusters grew approximately as $t^{1/3}$. Hydrogen clustering occurred initially over short correlation lengths, and for Fig. 9b the correlation length has grown to about 10 lattice parameters. When there were no interactions between hydrogen atoms and the minority metal atoms, a sharp interface was always observed around the clusters of hydrogen atoms.

Fig. 9c is a snapshot obtained after long times for a simulation with an attractive hydrogen–solute interaction. For the earliest times, clustering of hydrogen atoms occurred normally. When the correlation length for the hydrogen atom clusters became slightly larger than the mean separation between the minority solute atoms, the coarsening stopped. We believe the state of Fig. 9c is an equilibrium state because similar states were reached from initial distributions of hydrogen atoms that were either clustered or random. The reason for the arrest of coarsening is that energetically favorable metal–hydrogen bonds would have to be sacrificed for the hydrogen distribution to coarsen further.

The simple picture of an attractive interaction between a hydrogen atom and a neighboring solute atom is consistent with a lowering of the plateau pressure when solute is added to the alloy. However, a lowering of plateau pressure could also occur when the hydrogen–solute first-neighbor interaction is repulsive, but the hydrogen–matrix interaction becomes more attractive with solute concentration. Simulations of this case also evolve hydrogen distributions similar to those of Fig. 9c, and also show an arrest of coarsening.

These Monte Carlo simulations are inadequate for predicting precise hydrogen distributions or kinetics. For example, the simulations are two-dimensional and do not include elastic interactions. Nevertheless, the simulations do show some general trends of how local variations in the density of solute atoms can alter the distribution of hydrogen atoms. The arrest of coarsening caused by hydrogen–solute interactions is particularly interesting. For a fixed concentration of hydrogen, clustered into three-dimensional hydride (β -phase) zones, the surface-to-volume ratio is larger for smaller clusters. The surface energy therefore decreases as the clusters grow larger, and this provides the well-known driving force for coarsening. The driving force diminishes as the clusters grow larger. The hydrogen–solute interactions alter this picture of coarsening. At low concentrations the Sn solute atoms are distributed randomly over the 3g sites of the LaNi_5 crystal. A random distribution is not a uniform one, so there will

be statistical fluctuations in the local concentration of solute². When a solute concentration, c , is averaged over a number of sites, N , the fluctuations in c are approximately $(cN)^{-1/2}$. A cluster of β -phase will seek out the favorable fluctuations in concentration, but these become less favorable as the cluster grows larger. This solute–hydrogen interaction energy therefore favors small clusters, or perhaps ramified clusters. The balance between these two effects results in the arrest of coarsening at a particular cluster size.

5. Discussion

The isotherms in Fig. 1 show that the width of the plateau decreases with an increase in concentration, y , of Sn in the composition $\text{LaNi}_{1-y}\text{Sn}_y$. For example, approximately 60% of the low-energy hydrogen sites in the β -phase are available when $y=0.5$. When $y=0.5$, the Sn atoms occupy approximately 17% of the 3g sites, the other 3g sites being occupied by Ni atoms. Evidently, therefore, the addition of each Sn atom to a 3g site blocks approximately two sites from low-energy hydrogen adsorption in the β -phase. These two higher-energy sites could be those adjacent to Sn atoms, but this is beyond the level of detail that can be deduced from knowledge only of isotherms and hydrogen site occupancies in LaNi_5 [47,48]. The Sn reduces the energy of hydrogen absorption of other low-energy sites in the alloy, since Fig. 1 shows that the plateau pressure decreases upon alloying with Sn. From the change in equilibrium pressure by about a factor of 40 between binary LaNi_5 and $\text{LaNi}_{4.5}\text{Sn}_{0.5}$, we deduce that the chemical potential for a hydrogen atom is reduced by $1/2 k_B T \ln(40) = 1/2 \cdot 25 \cdot (3.7) = 46$ meV in the Sn-containing alloy. (Standard tables provide 40 meV [49]). These low-energy sites are presumably located somewhere in the vicinity of the Sn atoms, but again we cannot deduce the crystallographic sites from information from the isotherms. We can say, however, that the addition of Sn atoms causes the sites occupied by hydrogen in binary LaNi_5 to have large differences in the chemical potential for hydrogen atoms.

The origin of the reduction in absorption energy of the low-energy sites in LaNi_5 –Sn alloys has been attributed to an increase in the size of the interstitial sites where absorbed hydrogen is located, which is correlated with the expansion of the lattice parameter as Sn is substituted for Ni [39]. Our measurements show that the lattice parameter increases with Sn concentration [50] (cf. Fig. 3a–c). It seems reasonable that the energy penalty for inserting a hydrogen atom in the lattice is reduced when the interstitial

²The concentration itself depends on the volume of sampling. Consider the extreme cases — over the full crystal there will be a uniform concentration, whereas over an individual 3g site the solute concentration will be 0.0 or 1.0.

sites are larger, but the actual energy penalty depends on the amount of expansion caused by the hydrogen atom. This is obtained from our X-ray measurements on poisoned alloys. The expansion of unit cell volume after fully hydriding is found to be 24% for LaNi_5 , with 21% of this occurring discontinuously between the α - and β -phases. The expansions for $\text{LaNi}_{4.75}\text{Sn}_{0.25}$ is 21% for fully-hydrided material. With hydrogen depletion, however, Fig. 3d shows that the difference in specific volume between the α - and β -phases becomes as low as 12%.

The SANS intensity profiles have the same shape for all states of deuteration of the $\text{LaNi}_{4.75}\text{Sn}_{0.25}$. The log–log curves of Fig. 4 are nearly coincident when they are shifted vertically, meaning that they all have the same mathematical form, and differ only by a multiplicative constant. Because the additional scattering from the deuterium has the same shape as that from the alloy without deuterium, the density distribution of deuterium is the same as the density distribution of the alloy. The deuterium is homogeneous in the alloy, at least over the spatial range of SANS sensitivity. This homogeneity is also found for the fully-deuterated LaNi_5 alloy. The curves in Fig. 5 are nearly coincident, even without vertical shifts. This is as expected, since the only difference between the two samples is a small amount of Sn, which has a coherent scattering length intermediate between La and Ni. For fully-deuterated samples of $\text{LaNi}_{4.75}\text{Sn}_{0.25}$ and LaNi_5 , the SANS profiles are nearly the same, and have the same shape as for the undeuterated alloy itself. This suggests that all available sites for deuterium are filled in the fully-deuterated samples, and the deuterium concentration is homogeneous over the spatial range of the SANS sensitivity.

In partially-deuterated samples of LaNi_5 , however, there is a distinct difference in the shape of the SANS intensity (Fig. 6). The deuterium in these materials does not follow the density of the alloy, but has its own heterogeneities. These variations in deuterium density are on the order of 40–150 Å. Furthermore, the decrease in the slope of the Porod plot of Fig. 7 from -4 to -3 could indicate that these hydrogen-rich regions in the partially-deuterated samples of LaNi_5 have two-dimensional features [51]. The distribution of deuterium in the LaNi_5 is not homogeneous on the spatial scale of 40–150 Å.

Our SANS results show, to the best of our knowledge for the first time, differences in the distribution of hydrogen (deuterium) in LaNi_5 and LaNi-Sn . At spatial scales of tens of unit cells, the distribution of hydrogen in partially-hydrided LaNi-Sn is more homogeneous than in partially-hydrided LaNi_5 . Based on the measured isotherms, we argued that a Sn atom affects the chemical potential of an interstitial hydrogen atom by up to 40 meV. This is large compared to room temperature, and is arguably comparable to the $V_{\text{B-H}} = -1.2 k_{\text{B}}T$ used in the two-dimensional Monte Carlo simulations of Section 4. We therefore expect that as hydrogen is added to the material, the hydrogen atoms will first occupy the low-energy sites.

These are, presumably, sites somewhere in the vicinity of Sn atoms. Over the larger spatial scale where SANS is sensitive, the following energy argument suggests that a more homogeneous distribution of hydrogen atoms is expected. Assume again that the Sn atoms are distributed at random on the $3g$ sites. As described in Section 4, for a Sn concentration of c , the fluctuations in c are approximately $(cN)^{-1/2}$ when taken over a number N of $3g$ sites. With 23 \AA^3 associated with each $3g$ site, the number of $3g$ sites in a sphere of diameter 50 Å is approximately 3000, so the fluctuations in this number are $(0.18 \cdot 3000)^{-1/2}$, or about 4%. Using a variation in chemical potential of hydrogen of 40 meV, these fluctuations in hydrogen concentration correspond to fluctuations in chemical potential of only about 2 meV per hydrogen atom in the cluster, which is small compared to room temperature. We therefore expect the distribution of hydrogen in $\text{LaNi}_{4.75}\text{Sn}_{0.25}$ to tend to be uniform on spatial scales of 50 Å or larger, in spite of the local variations in chemical potential in hydrogen sites near Sn atoms.

On the other hand, without solute atoms to cause local variations in the chemical potential of hydrogen, the distribution of hydrogen in binary LaNi_5 should be affected primarily by the surface energy of the hydride/matrix interface, modified by elastic interactions between the hydride zones. Our SANS curves of partially-deuterated LaNi_5 suggest the hydride zones are two-dimensional. A plate is a common morphology for an elastic precipitate in an anisotropic crystal. Previous SANS work has shown similar evidence for Pd hydride [52]. Planar defects have been reported by TEM observations on LaNi_5 [53].

The spatial scales of these hydrided zones, or rather the correlation length for the hydrogen density fluctuations in partially-hydrided binary LaNi_5 , are of order 40–150 Å. With a linear strain of 5–7% from full hydriding, the variation of hydrogen concentration from 0 to 100% over distances from 40 to 150 Å results in a large strain gradient of 0.2–1% across a unit cell. It is not surprising that this large strain gradient could lead to the generation of dislocations or other crystalline defects that could initiate fracture. We propose that the effect of Sn atoms on smoothing the mesoscopic hydrogen concentration profile is why LaNi-Sn sustains less microstructural damage than binary LaNi_5 . Perhaps this is responsible for the improved cycle life of solute-modified LaNi_5 for application as both gas storage and electrochemical cell materials.

6. Conclusion

We performed a comparative study of hydrogen distributions and strains in LaNi_5 and the alloy $\text{LaNi}_{4.75}\text{Sn}_{0.25}$, which has been shown to have a superior cycle life to binary LaNi_5 for hydrogen storage and in electrochemical cells. X-ray diffractometry showed that the

overall volume dilatations during full hydriding were approximately the same for the two alloys, but the unit cell volume of the β -phase (the hydride) in $\text{LaNi}_{4.75}\text{Sn}_{0.25}$ became closer to that of the matrix α -phase during loss of hydrogen. Gas-phase isotherms show that the Sn atoms cause large changes in the chemical potential at sites of hydrogen occupancy, with some sites having low and other sites having high chemical potentials. We used generic hydrogen–solute interactions in Monte Carlo simulations and physical arguments to show why the normal coarsening behavior of hydride zones will be altered, and even arrested, by hydrogen–solute interactions. Interactions between Sn and deuterium atoms provide a mechanism for homogenizing the deuterium distribution over mesoscopic spatial scales somewhat larger than a unit cell.

Small angle neutron scattering shows that the distribution of deuterium in partially-deuterated $\text{LaNi}_{4.75}\text{Sn}_{0.25}$ is more homogeneous than in partially-deuterated LaNi_5 , at least on the spatial scale of 40–150 Å. The deuterium distribution is found to be the same in fully-deuterated LaNi_5 and $\text{LaNi}_{4.75}\text{Sn}_{0.25}$, and this distribution matches well the density distribution of the sample itself (i.e. the deuterium distribution is homogeneous). We suggest that a more homogeneous deuterium distribution could suppress the internal stresses upon hydriding that cause defect formation and fracture.

Acknowledgements

The authors thank Dr R.C. Bowman, Jr. for discussions and advice, and Dr J.G. Barker for assistance with the SANS measurements. This work was supported by DOE through Basic Energy Sciences Grant DE-FG03-00ER15035.

References

- [1] J.G.G. Willems, K.H.J. Buschow, *J. Less-Common Met.* 129 (1987) 13.
- [2] T. Sakai, M. Matsuoka, C. Iwakura, in: K. Gschneidner, Jr, L. Eyring (Eds.), *Handbook on Physics and Chemistry of Rare Earths*, Vol. 21, Elsevier, Amsterdam, 1994, p. 133.
- [3] R.L. Cohen, K.W. West, J.H. Wernick, *J. Less-Common Met.* 70 (1980) 229.
- [4] R.L. Cohen, J.H. Wernick, *Science* 214 (1981) 1081.
- [5] R.L. Cohen, K.W. West, *J. Less-Common Met.* 95 (1983) 15.
- [6] A.R. Miedema, P.F. de Chatel, F.R. de Boer, *Physica* 100B (1980) 1.
- [7] T. Sakai, K. Oguru, H. Miyamura, N. Kuriyama, A. Kato, H. Ishikawa, C. Iwakura, *J. Less-Common Met.* 161 (1990) 193.
- [8] T. Sakai, T. Hagama, H. Miyamura, N. Kuriyama, A. Kato, H. Ishikawa, *J. Less-Common Met.* 172–174 (1991) 1175.
- [9] T. Sakai, H. Yoshinaga, H. Miyamura, H. Ishikawa, *J. Alloys Comp.* 180 (1992) 37.
- [10] T. Sakai, H. Miyamura, N. Kuriyama, H. Ishikawa, I. Uehara, *Z. Phys. Chem.* 183 (1994) 333.
- [11] J.G.G. Willems, *Philips J. Res.* 39 (Suppl. 1) (1984) 1.
- [12] A. Anani, A. Visintin, K. Petrov, S. Srinivasan, J.J. Reilly, J.R. Johnson, R.B. Schwarz, P.B. Desch, *J. Power Sources* 47 (1994) 261.
- [13] M.P. Sridhar Kumar, W. Zhang, K. Petrov, A.A. Rostami, S. Srinivasan, G.D. Adzic, J.R. Johnson, J.J. Reilly, H.S. Lim, *J. Electrochem. Soc.* 142 (1995) 3424.
- [14] G.D. Adzic, J.R. Johnson, J.J. Reilly, J. McBreen, S. Mukerjee, M.P. Sridhar Kumar, W. Zhang, S. Srinivasan, *J. Electrochem. Soc.* 142 (1995) 3429.
- [15] A. Percheron-Guégan, M. Latroche, J.C. Achard, Y. Charbre, J. Bouet, *Electrochem. Soc. Proc.* 94–27 (1994) 196.
- [16] F. Meli, A. Züttel, L. Schlapbach, *J. Alloys Comp.* 202 (1993) 81.
- [17] F. Meli, A. Züttel, L. Schlapbach, *Z. Phys. Chem.* 183 (1994) 371.
- [18] F. Meli, A. Züttel, L. Schlapbach, *J. Alloys Comp.* 231 (1995) 639.
- [19] B.V. Ratnakumar, C.K. Witham, G. Halpert, B. Fultz, *J. Electrochem. Soc.* 141 (1994) L89.
- [20] B.V. Ratnakumar, C.K. Witham, R.C. Bowman, Jr, A. Hightower, B. Fultz, *J. Electrochem. Soc.* 143 (1996) 2578.
- [21] B.V. Ratnakumar, S. Surampudi, B. Fultz, C. Witham, R.C. Bowman, Jr, A. Hightower, NASA Tech Briefs, August 1998, pp. 60–61.
- [22] C.K. Witham, B. Fultz, B.V. Ratnakumar, R.C. Bowman, Jr, in: P.D. Bennett, T. Sakai (Eds.), *Proc. Symp. on Hydrogen and Metal Hydride Batteries*, The Electrochemical Society, Inc., 1995, 94–27. ISBN: 1-56677-086-6, p. 68.
- [23] P.H.L. Notten, R.E.F. Einerhand, J.L.C. Daams, *J. Alloys Comp.* 231 (1995) 604.
- [24] P.H.L. Notten, in: F. Grandjean, G. Long, K.H.J. Buschow (Eds.), *Interstitial Metallic Alloys*, Kluwer, London, 1995, p. 151.
- [25] O.A. Petrii, S.Y. Vasina, I.I. Korobov, *Russ. Chem. Rev.* 65 (1996) 181.
- [26] P.H.L. Notten, R.E.F. Einerhand, J.L.C. Daams, *J. Alloys Comp.* 210 (1994) 221.
- [27] T. van Waldkirch, P. Zurcher, *Appl. Phys. Lett.* 33 (1978) 689.
- [28] A.H. Boonstra, T.N.M. Bernards, *J. Less-Common Met.* 161 (1990) 245.
- [29] A.H. Boonstra, T.N.M. Bernards, G.J.M. Lippits, *J. Less-Common Met.* 159 (1990) 327.
- [30] D. Chartouni, F. Meli, A. Züttel, K. Gross, L. Schlapbach, *J. Alloys Comp.* 241 (1996) 160.
- [31] P.H.L. Notten, J.L.C. Daams, R.E.F. Einerhand, *J. Alloys Comp.* 210 (1994) 233.
- [32] P.H.L. Notten, J.L.C. Daams, A.E.M. De Veirman, A.A. Staals, *J. Alloys Comp.* 209 (1994) 85.
- [33] R.C. Bowman, C. Luo, C.C. Ahn, C.K. Witham, B. Fultz, *J. Alloys Comp.* 217 (1995) 185.
- [34] S. Mukerjee, J. McBreen, J.J. Reilly, J.R. Johnson, G. Adzic, K. Petrov, M.P.S. Kumar, W. Zhang, S. Srinivasan, *J. Electrochem. Soc.* 142 (1995) 2278.
- [35] M.L. Wasz, P.B. Desch, R.B. Schwarz, *Phil. Mag.* 74 (1996) 15.
- [36] M.L. Wasz, R.B. Schwarz, *Mater. Sci. Forum* 225–227 (1996) 859.
- [37] M.L. Wasz, R.B. Schwarz, S. Srinivasan, M.P.S. Kumar, *Mater. Res. Soc. Symp. Proc.* 393 (1995) 237.
- [38] S. Luo, W. Luo, J.D. Clewley, T.B. Flanagan, L.A. Wade, *J. Alloys Comp.* 231 (1995) 467.
- [39] S. Luo, J.D. Clewley, T.B. Flanagan, R.C. Bowman, L.A. Wade, *J. Alloys Comp.* 267 (1998) 171.
- [40] J.R. Johnson, J.J. Reilly, *Inorg. Chem.* 17 (1978) 3103.
- [41] F. Izumi, T. Ikeda, *Mater. Sci. Forum* 198 (2000) 321.
- [42] B. Fultz, *J. Chem. Phys.* 87 (1987) 1604.
- [43] H. Ouyang, B. Fultz, *J. Appl. Phys.* 66 (1989) 4752.
- [44] T.F. Lindsey, B. Fultz, in: B. Fultz, R.W. Cahn, D. Gupta (Eds.), *Diffusion in Ordered Alloys*. TMS Monograph Series, Warrendale, 1993, pp. 91–106.
- [45] N. Metropolis, A.W. Rosenbluth, M.N. Rosenbluth, A.H. Teller, E. Teller, *J. Chem. Phys.* 21 (1953) 1087.
- [46] Y. Limoge, J.L. Bocquet, *Acta Metall.* 36 (1988) 1717.
- [47] C. Lartigue, A. Percheron-Guégan, J.C. Archard, J.L. Soubeyrou, *J. Less-Common Met.* 113 (1985) 127.

- [48] P. Thompson, J.J. Reilly, L.M. Corlis, J.M. Hastings, R. Hemplemann, J. Phys. F Met. Phys. 16 (1986) 675.
- [49] R.D. McCarty, J. Hord, H.M. Roder, in: Selected Properties of Hydrogen, NBS Monograph 168, US Government Printing Office, Washington, DC, 1981, pp. 6-130–6-269. W.E. Forsythe (Ed.), Smithsonian Physical Tables, 9th ed., Smithsonian Institute, Washington, 1964.
- [50] C.K. Witham, Ph.D. Thesis, Materials Science, California Institute of Technology, 1999.
- [51] B. Fultz, J.M. Howe, Transmission Electron Microscopy and Diffractometry of Materials, Springer, Heidelberg, 2001, Chapter 8.
- [52] B.J. Heuser, J.S. King, W.C. Chen, J. Alloys Comp. 292 (1999) 134.
- [53] A.E.M. De Veirman, A.A. Staals, P.H.L. Notten, Phil. Mag. A 70 (1994) 837.